Sustainable Energy & Fuels

Interdisciplinary research for the development of sustainable energy technologies

Accepted Manuscript

This article can be cited before page numbers have been issued, to do this please use: P. Mishra, R. Zhang, P. Wang, Y. Geng, D. Li, Q. Xu, J. W. Wong and J. Zhao, *Sustainable Energy Fuels*, 2026, DOI: 10.1039/D5SE01709B.

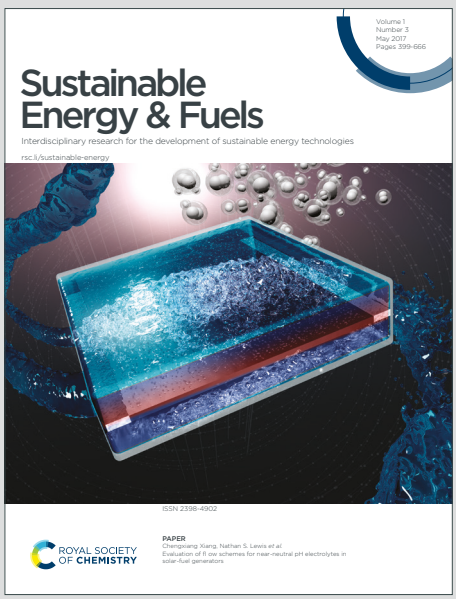

View Article Online
DOI: 10.1039/D5SE01709B

Genome-Resolved Insights into Ni/Fe_2O_3 Nanocatalyst-Enhanced Dark Fermentative Hydrogen Production from Food Waste

*Puranjan Mishra [a], Ruilong Zhang [a], Peixin Wang[a], Yiqi Geng [a], Dongyi Li [ab], Qiuxiang Xu[b], Jonathan W.C. Wong [b], Jun Zhao [a,c] **

[a] Sino-Forest Applied Research Centre for Pearl River Delta Environment, Department of Biology, Hong Kong Baptist University, Hong Kong, China

[b] Research Center for Eco-Environmental Engineering, Dongguan University of Technology, Dongguan, Guangdong 523808, China

[c] Institute of Advanced Materials, Hong Kong Baptist University, Hong Kong, China

* Corresponding author: Jun Zhao: zhaojun@hkbu.edu.hk

Abstract

Ni/Fe_2O_3 nanocatalysts are effective in increasing the yield of fermentative biohydrogen (H_2).production; however, the underlying microbial and metabolic mechanisms remain insufficiently understood. In this study, food waste (FW) based dark fermentative (DF) H_2 production was significantly improved by the addition of a synthesized Ni/Fe_2O_3 nanocatalyst, achieving a increase H_2 yield up to 55.65% compared to the control. The presence of Ni/Fe_2O_3, improved system pH-stability, conductivity, and electron transport capacity, which simultaneously accelerated the microbial metabolism in DF-system. Genome-centric metagenomic analysis revealed that the catalyst reshaped the microbial community and metabolic functions by promoting Clostridium species as dominant H_2-producing bacteria and enriching genes associated with carbohydrate metabolism, complex saccharide hydrolysis, nutrient transport, glucose phosphorylation, and electron transfer pathways. These findings uncover a previously unrecognized catalytic role of Ni/Fe_2O_3 in regulating microbial community structure and metabolic pathways, providing genome-level insights into catalyst–microbe interactions and offering a mechanistic foundation for advancing food waste–derived H_2 production.

Keywords: Biohydrogen; Nanoparticle; Ni/Fe_2O_3; Metagenomics; Food waste

View Article Online
DOI: 10.1039/D5SE01709B

1. Introduction

Global carbon emissions are driven by the increasingly conventional use of fossil-based fuels to meet energy demand with the growing world population, intensifying the research for sustainable bioenergy production [1]. The adoption of an integrated system combining dark fermentative (DF) biohydrogen production with advancement in nanotechnology to enhance the fermentative process is essential for achieving higher bioenergy production. Hydrogen (H_2), with its high calorific value (120-142 MJ kg^{-1}), is regarded as a green and sustainable fuel and approaches to produce H_2 from biomass, has become a significant research focus due to its potential for increasing bioenergy efficiency and sustainability [2]. Leveraging the integrations of materials-nanotechnology and DF technology [3], the biological conversion of nutrient rich organic waste such as food waste [4] (which contains almost 30% of organics *e.g.* complex polysaccharides, proteins, and lipids and claimed its regular generation of more than 2000 t/d [5]) into H_2 has immense potential to increase resiliency and sustainability [6] .

H_2 production, in particular via DF from FW involved primarily 'solubilization' and 'hydrolysis' of macromolecules into monosaccharides and amino acids. Later biologically it converted into acetate (C_2-H_{Ac}), butyrate (C_4-H_{Bu}) and other short-chain volatile fatty acids (VFA) with simultaneous production of H_2 depending upon the metabolic pathways followed by microorganism (pyruvate-ferredoxin oxidoreductase pathway (PFOR) or pyruvate-formate lyase pathway (PFL)[7]. Although the DF process is ubiquitous and takes place in natural environment and engineered systems [8], the conversion the complex organic macromolecules into H_2 remains challenging due to low yield and productivity (as so "Thauer limit" 4 mol of H_2 can be produced per mole of $C_6H_{12}O_6$) [9]. The DF system has several significant environmental benefits to produce H_2, thus numerous efforts were dedicated previously to promote the H_2 metabolic process performance [10]. Engineered metallic nanoparticles have demonstrated enhanced electrocatalytic activities[11], making them highly effective in anaerobic processes aimed at optimizing the biological degradation of organic waste[7]. Metallic catalysts serves as an efficient catalytic activities to promote DF based bioconversion of waste to H_2 (by facilitating hydrolysis, improving solubility, and enriching hydrolytic bacteria within the microbial community [12]. In recent years, a series of Metallic catalysts has been explored including metal oxides and their derivatives to accelerate the H_2 production and microbial metabolic pathways [7, 13] and the quest to find a suitable nanocatalyst is expanding exponentially. Previous investigations revealed the stimulating effect of single metallic nanoparticles on DF based H_2 production and found to be a connection with type, size and exposures forms of nanoparticles [14]. These catalysts elevate the DF-process performances through following manners: (a) influencing the production activities of vital Hydrogenases enzymes [15] (b) facilitating the electron transfer between electron carriers [16](c) facilitating the substrate biodegradability [17] (d) facilitating cytoprotective properties behaviors of anaerobes[18] etc.

View Article Online
DOI: 10.1039/D5SE01709B

It is considered that the incorporation of the nanocatalyst significantly enhances DF compared to bulk one, which attributed to their quantum size effect and high surface area, which increases electron adsorptions and contributes to efficient electron exchange between catalysts and DF microbial enzymes (NAD, FAD etc.) [19]. Exemplifying this, 'Iron' a vital element for enzymes ([Fe-Fe] hydrogenase, [Fe-Ni] Hydrogenases, dehydrogenases, reductase etc.), has been reported for its nanosized form for the catalytic activity in DF based H_2 production system [20]. Functions of nanocatalyst as reducing agent lowers the system's oxidation-reduction potential (ORP) and considerably enhance the hydrolysis of organic waste by fostering the anaerobic microenvironment of DF-system [20]. Fe-NPs have been reported on their positive effect on the DF-system based H_2 production and presumed their function relying on shifting of intermediate metabolites production towards a higher C_2-H_{Ac} to C_4-H_{Bu} ratio, favoring H_2 production [21]. The morphological study of the catalyst reported the higher cell aggregation in the presence of Fe_2O_3 NPs due to formation of bacterial nanowire, which played an important role electron transfer system during DF-system [22]. Besides, Nickle (Ni), the element possessed as cofactors of hydrogenase along with other vital enzymes which are involved in energy metabolic pathways, and its adequate dosages elevate microbial growth and thereby H_2 productivity [23]. Study shows, the Ni/FeO_x nanoparticles has a bulk oxido-reductive potential as high as high 1.2 S^{-1} at an overpotential of 300mV, while the higher catalytic activity of Ni/FeO_x is well established [24], there is vivid debate like the activity, especially whether Ni/FeO_x is an active catalyst for H_2 production in DF-system. Zang et al, reported that *Eichhornia crassipes's* extracted NiO NPs possess the ability to improve the H_2 productivity by 47.29% compared with control in DF-system [25]. Hydrogenase, a key enzyme of DF-system that catalyzes NADH categorizes into [Ni-Fe] and [Fe-Fe] hydrogenases exhibits central active metal, and formal was ubiquitous in microbes than the latter [26]. Ferredoxin hydrogenase, important in DF-system, Yang et al [27] and Li et al [23] reported the active participation of iron and nickel composite in boosting the synthesis of ferredoxin hydrogenases in DF-system based H_2 production employed with La—Fe oxides and Ni-Co oxides NPs, respectively.

The DF-system based H_2 production, which is associated with microbial functional dynamics, is complex, and still has a long way to go to become competitive biofuel technology for H_2 generation at commercial level. Although, literature reported on the modulating impressions of nano-sized catalysts on H_2 production via DF-system [28], use of bimetallic NPs and cautious interpretations of cross-microbial dynamics analysis and performance analysis are yet to be explored, particularly in systems augmented with Ni/Fe_2O_3 nanocatalyst.

Besides, the comprehensive analysis of mechanisms underlying Ni/Fe_2O_3 catalyst in microbial populations while using real FW in DF-system remains unfolded. Therefore, understanding the mode of action of Ni/Fe_2O_3 on DF-system using high throughput metagenomics, can lead to clear picture on Ni/Fe_2O_3-

View Article Online
DOI: 10.1039/D5SE01709B

induced regulatory mechanism of complex microbiome system followed by pathways involved in the cellular process and organismal systems, metabolic pathways are still needed to be explored. The purpose of this study was therefore reporting new insight at the taxio-metagenomic level coordination lading bioconversion of FW to H_2 in response to prepared Ni/Fe_2O_3 catalyst using FW in a DF-system. Beginning with the preparation of novel Ni/Fe_2O_3 composite with excellent catalytic ability to increase biological conversion of FW into H_2 in a controlled DF-system, the characteristics of Ni-modified Fe nanocatalyst were comprehensively revealed by series of characterizations using XRD, XPS, FESEM, and TEM. The parametric-performance characteristics were assessed by employing Ni/Fe_2O_3 in DF-system, where the performance impact was analyzed at various level following; (a) the influence of Ni/Fe_2O_3 on the hydrolysis and solubilization of FW, (b) transformation of FW to H_2, Electron transfer system, VFA and (c) on the activity of key microbial dynamics at taxio-metagenomic level were investigated to explore possible reason for Ni/Fe_2O_3 catalyzing H_2 production at genetic level within microbial population.

2. Material and methods

2.1 Catalyst Preparation

The Ni/Fe_2O_3 NPs were prepared (on molar ratio basis) by modified co-precipitation method, based on methodology previously reported in our previous literature [28]. The procedure to prepare catalyst, in aqueous iron nitrate nonahydrate solution (In 100 mL H_2O, 0.1 mM Fe $(NO_3)_3(H_2O)_9$, sigma-Aldrich), 0.05mM of Ni $(NO_3)_2.6H_2O$ (Sigma-Aldrich) fully dissolved in a continuous stirring system followed by precipitation using drop wise addition of 1 M NaOH (adjusted till 10-11). Upon pH adjustment, reaction mixture was seeded by heating to 80 ºC with stirring (450 rpm) for 3 h. The resulting slurry was properly deionized by H_2O and ethanol; following this the slurry was dried at 60 ºC for 16 h to allow complete evaporation of water. The resulting material was ground prior to calcination (450 ºC, 2h, 5 ºC min^{-1})[28].

2.2 Catalyst Characterization

The structure of catalyst was determined by power X-ray diffraction using cu Kα radiation source, operating at 40 keV and 40 mA. X-ray photoelectron spectroscopy was made to analyze composition and redox states of catalyst, and the atom distribution was observed using TEM-EDS. The surface morphologies of the catalyst were studied using field emission scanning microscopy (FESEM, Zeiss) operated at an electron voltage of 5 KV. Transmission electron microscopy (TEM) was used to configure the internal morphologies operated under an acceleration voltage of 200 kV with tecnaiG2 FEI Co TEM.

2.3 Food waste and seed sludge

View Article Online
DOI: 10.1039/D5SE01709B

The synthetic FW was prepared in Lab (constituent of FW describe in *Supporting Information*), and before experiments the FW was grounded to the slurry with dilution of Tap water to final TS and pH. The seed sludge with heat pretreatment was used an inoculum for DFHP system[29], adopted from Sai kung sewage wastewater treatment plant, Sai Kung, Hong Kong and stored at 4 ºC to prevent degradation. The characteristics of seed sludge and FW are mentioned in *Supporting Information (Section 1)*. The enrichment of H_2 producing microbes and to restrain the methanogens, the sludge was incubated at 90 ºC for 2h in water bath system [28].

2.4 Ni/Fe_2O_3 role in solubilization and hydrolysis of FW

DF-system process subjecting FW as substrate is critically related to solubilization and hydrolysis [12]. Herein, the solubilization and hydrolysis impact at various doses of Ni/Fe_2O_3 ranged from 50 to 500 mg/L were carried out using FW, where the DF lasted for 3 days. The procedures detailed are supplied in the *Supporting Information (Section 2a and b SI)*.

2.5 Ni/Fe_2O_3 role in DF-system based H_2 production from FW

The experiment on Ni/Fe_2O_3 affecting the H_2 production and microbial community at their metabolic and genomic level was carried out using identical serum bottles with working volume of 120 mL. The FW slurry with an initial TS of 10 g/L was prepared using Tap water and 10% heat-pretreated sludge [30] was added. The mixture was divided equally by 18 reactors, which belong to six groups with three samples each, to study the effect of H_2 production and microbial taxio-metagenomic analysis. On the basis of Ni/Fe_2O_3 Catalysts doses employed to DF-process, the reactors were annotated as control, T-50, T-100, T-200, T-300 and T-500 mg/L of Ni/Fe_2O_3 , respectively. The initial pH of each serum bottle was adjusted to 5.5 ± 0.2. After being flushed with nitrogen gas to remove O_2 for 2 min, all the serum bottles were capped properly with rubber stopper, sealed and placed in an orbital shaker with a speed of 180 rpm and incubation temperature of 35 ± 2 ºC for 3 days. Final pH, conductivity (Eh), were measured post DF-system. Liquid samples were collected from the serum bottles using a 5 mL gas syringe, filtered through a 0.2 µm membrane and stored in a 2 mL GC vial at 4 ºC for physio-chemical analysis. Volumetric analysis of produced H_2 gas was calculated from the head space measurement, fraction of H_2 gas in the heads-space of the gas composition, and the pressures exerted in each serum bottle.

2.6 Ni/Fe_2O_3 catalysts 's role in Electron Transport System

To analyze the electro-catalytic behavior of Ni/Fe_2O_3 catalysts on microbial activity during DF-system, ETS activity was analyzed by performing modified (2-(p-idophenyl)-3(-(p-nitrophenyl)-5-phenyltetrazolium chloride (INT) assay [31]. In brief, after 4 days of fermentation in seven groups of identical

View Article Online
DOI: 10.1039/D5SE01709B

reactors with corresponding levels of Ni/Fe_2O_3-5% (control, 50 mg/L, 100 mg/L, 150 mg/L, 200 mg/L, 300 mg/L, 500 mg/L), the samples were collected out from each reactor and determined the electron transport system activity. The detailed methodology to assess the ETS activity is mentioned in *Supporting Information (Section 2(c) SI)*.

2.7 DNA extraction, Sequencing and Bioinformatics analysis

Microbial community and metagenomic analysis of the control (no-Ni/Fe_2O_3) and a representative experiential group (200 mg/L Ni/Fe_2O_3: based on higher observed H_2 yield) was carried out using 16 sRNA high-throughput gene sequencing. For these two groups, 5 mL of the 3 days fermented sample were taken out from the three parallel serum bottles from test group and mixed and then stored in the refrigerator at -80 ºC. Total DNA from both the samples was extracted and quantified. V4-V% region of 16sRNA of each sample was amplified using PCR. The employed methods and parameters were followed as described in literature [32]. The Sequence content Quality score across (*Table SA1-SA3 SI*) all bases observed for control and test samples is highlighted with detailed information on sequencing and metagenomic analysis procedures is described in *Supporting Information (Section 2(d) SI)*. All the assays were conducted in triplicate and the results as error bar (± Standard deviation). An analysis of variance (ANOVA) was used to test the significance pf the results, and p, 0.05 was considered statistically significant.

2.8 Sampling, analysis and analytics

The Total Solids (TS), Volatile Solids (VS), pH, of FW and Sludge inoculum in the experiments were analyzed using APHA standard Method 2540 [33]. The constituents of FW (C, H, N, and S) were analyzed using ELEMENTAR Vario MARCO cube Analyzer (Sci Focus Lmt. HongKong). The conductivity of DF-systems (pre and post fermentation) was measured using Portable Digital lab Conductivity Meter Dds-11c (Puchun Instruments, Shanghai). Where, the Probe of the conductivity meter were calibrated using 0.01 M KCl, 1413 µS/cm at 25ºC to ensure authenticity of observed conductivity. Fraction analysis of produced gas was analyzed by Gas chromatography (GC-8500, perkin, USA) (equipped with TCD detector; column (SS350A) and molecular sieve (80/100 mesh). The soluble metabolites analysis was determined using high performance liquid chromatography (HPLC-Agilent-1200, USA). The operational conditions applied for GC and HPLC, and calculation for the H_2 magnitude were referred to in our previous experiment [28]. Prior to analysis, the samples from the ceased H_2 production system were collected and centrifuged at 6000 rpm for 10 min and filtered through a 0.45 µM membrane filter of soluble metabolites analysis.

3. Results and Discussion

3.1 $NiFe_2O_3$ synthesis and characteristics

View Article Online
DOI: 10.1039/D5SE01709B

Brownish powdery mixture was obtained after final calcination of starting material $Fe(NO_3)_3(H_2O)_9$ and $Ni(NO_3)_2.6H_2O$ with the molar ratio of 0.01mM (Iron precursor):0.005mM (Ni precursor). Scanning electron microscopy images Figure 1 (a-c) showed the crystalline morphologies ranges in nanosized. The XRD patterns (Figure 1g) of Ni/Fe_2O_3 with distinct diffraction peaks located and which can be assigned to be the (111), (200), (311), (400), (511), and (440) crystal plane reflection of a face -central cubic nickel phase (JCPDS 54-0964). However, a light shifting at (220) and (311) corresponds to Fe_2O_3 (39-1346) in Ni/Fe_2O_3 composite could be observed, implying the substitutional associations between iron and nickel particles. Scherrer analysis [28] of diffraction peaks (311) for Fe_2O_3 (39-1346) suggested the grain size of 0.251 nm at 2θ of 35.630, while the $Ni_{0.05}Fe_{0.1}$ composite indicated the grain size of 2.5130 nm along the 35.699 (2θ) crystallographic axis direction [34], consistent with the results observed from SEM (Figure 1c). The observed diffractions peaks illustrated that Ni/Fe_2O_3 catalysts has a proportion of crystalline regions, thus making the material more stable. SEM images in Figure 1c of Ni/Fe_2O_3 catalysts showed the appearance of irregularly agglomerated shapes. The particles were relatively uniform and smooth and were slightly agglomerated [35]. Acquiring the elemental composition of Ni/Fe_2O_3, XPS spectrum, Figure 1(i-k) reveals the existence of Ni, Fe and O and this is not only consistent with XRD but also suggested the purity of the Ni/Fe_2O_3 Catalysts . The XPS survey orbital spectrum peaks at 529, 780 and 855 eV confirmed the existence of O1s , Fe2p and Ni2p respectively [23]. The high-resolution TEM images of nanoparticles in Figure 1(d-f) presented 0.250 lattice fringes, which can be attributed to the (311) lattice plane of the Ni-Fe composite [36], in line with XRD results. The XPS oxygen spectrum (SI Figure S1) reveals different oxygen components and was labeled as O1, O2 and O3, respectively. The O1 corresponds to the typical metal-oxygen bond in the oxides with a binding energy value of 529.6 eV, while O2 and O3 peaks at 530.9 eV and 532.7 were oxygen vacancies [37]. These vacancies are important to resistance of proton movement and acceleration of the shuttling in the surface layer [38]. Further, the Ni 2p spectrum exhibited peaks at 854.8 eV and 872.6 eV of $2p_{3/2}$ and $2p_{1/2}$, respectively depicting the Ni^{3+} and Ni^{2+} (Figure 1k), respectively. The refraction peaks at 854.8 eV and 856.3 eV ascribes the appearance of Ni^{3+} and Ni^{2+} in $Ni2p_{3/2}$ orbital. Similarly, the refraction peaks at 871.9 eV and 872.7 eV ascribe the appearance of Ni^{3+} and Ni^{2+} in $Ni2p_{1/2}$ orbital, which are in line with literature [39, 40]. The Fe 2p profiles with two peaks at 710.8 eV and 724.4 eV for Fe $2p_{3/2}$ and Fe $2p_{1/3}$, respectively, indicated the existence of Fe^{2+} and Fe^{3+}, Figure 1j. The peaks at 709.9 eV and 712 eV ascribe the presence of Fe^{2+} and Fe^{3+} which were coexisted in Fe $2p_{3/2}$ spin. Similarly, the refractive peaks at 723.2 eV and 725.5 eV ascribe the presence of Fe^{2+} and Fe^{3+} which were coexisting at Fe $2p_{1/2}$ spin [41, 42]. The nature of charge on metal ions is critical for the systematic improvement in the E_h of the Ni/Fe to a system [43]. Based on observed peaks areas for Ni^{2+}, Ni^{3+}, Fe^{2+} and Fe^{3+}, the Ni/Fe_2O_3 Catalysts exhibited the bivalency with Ni^{2+}/Ni^{3+} and Fe^{2+}/Fe^{3+} ratio of 1.07 and 0.40, respectively.

View Article Online
DOI: 10.1039/D5SE01709B

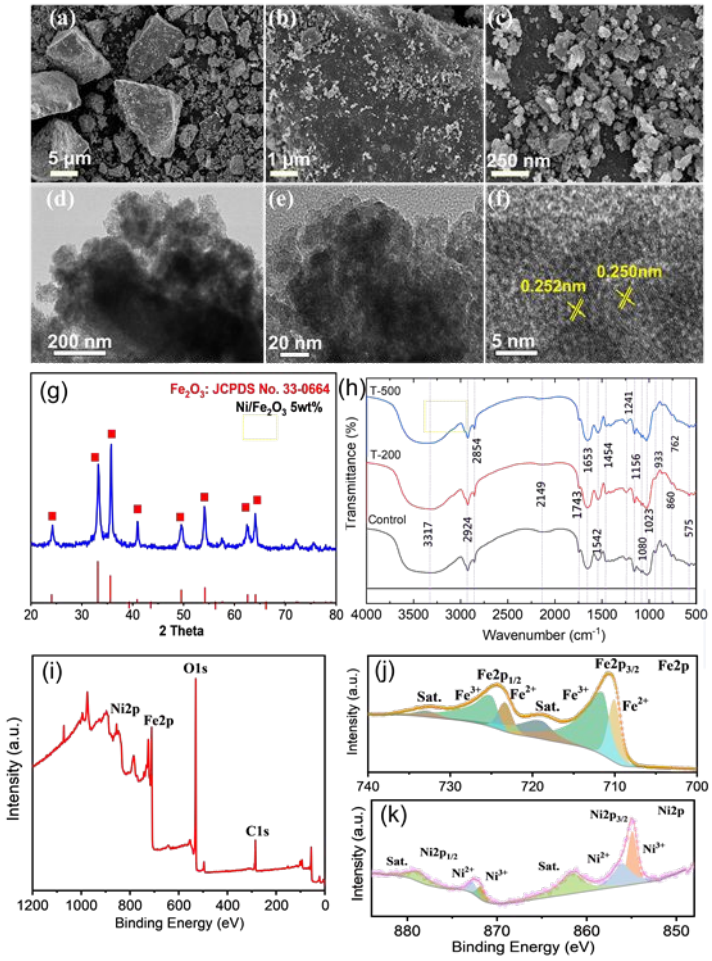

Figure 1. (a, b) Low magnification and (c) high-resolution SEM image of representatives Ni/Fe_2O_3-5%. (d) Low-magnification and (e, f) high-resolution images of corresponding TEM images of Ni/Fe_2O_3-5% (g) XRD spectrum of representative Ni/Fe_2O_3-5% sample (h) FT-IR spectrum of food waste sampled from post anaerobic biohydrogen production enriched with and without Ni/Fe_2O_3. (i) Full XPS spectrum of representative Ni/Fe_2O_3-5% sample (j) High resolution XPS spectra of Fe_{2p}. and (k) High resolution XPS spectra of Ni_{2p}

3.2 Ni/Fe_2O_3 facilitated FW solubilization and hydrolysis

The FW existed in its complex form, and therefore, the extent of hydrolysis and its solubilization for its disintegration into the simplest form of nutrients accompanied by releasing into the liquid broth for substantial mass transfer between medium to microcosm is important to significant H_2 production from DF-system [12]. Figure 2(a-b) depicts the soluble protein and polysaccharides concentration after fermentation in response to different concentrations of Ni/Fe_2O_3 added to the FW-based DF-system. In Figure 2a, at the Ni/Fe_2O_3 level of 50, 100, 150, 200, 300 and 500 mg/L, the soluble polysaccharide concertation percentage was 71.26%, 74.15%, 77.25%,77.91%, 65.62%, and 65.98%, showing a significant variations ($p=0.02$, <

View Article Online
DOI: 10.1039/D5SE01709B

0.05), whereas comparing with the control (71.23%) the test-medium with 200 mg/L of Ni/Fe_2O_3 appeared 7% increased and evidence more soluble carbohydrates release to the DFHP system. A similar trend is observed for soluble protein analysis. Where, at the Ni/Fe_2O_3 level of 50, 100, 150, 200, 300 and 500 mg/L, the soluble protein percentage was 32.96%, 32.11%, 38.06%, 33.17%, 30.19%, and 28.28%, showing a significant variation in concentrations ($p=0.02$, $p < 0.05$). Compared with the control system (28.07%), DF-system increased to 200 mg/L of Ni/Fe_2O_3 resulting in a 10% increased solubility of protein to the system. Hydrolysis of FW refers to the degradation of polysaccharides (macro molecular saccharides) and soluble protein into monosaccharides and amino acids, respectively [44]. Figure 2b shows the degree of hydrolysis in % using BSA and Cellobiose as model protein and carbohydrate in responses to different dosages of Ni/Fe_2O_3 ranging from 50 mg/L to 500 mg/L in DF-system after 3 days of incubation. In the control system, where no Ni/Fe_2O_3 was added, the percentage of BSA and Cellobiose hydrolysis was observed as 47.25% and 92.24%, respectively. This suggests that anaerobic sludge contains a considerable range of microbiomes able to hydrolyze the complex low molecular disaccharides. The decline degree in food waste hydrolysis observed at Ni/Fe_2O_3 nanoparticle concentrations above 300 mg/L can be explained by two primary factors. First, at high concentrations, the nanoparticles exert a toxic effect on hydrolytic bacteria, inducing significant oxidative stress that damages essential cellular components like DNA, proteins, and cell membranes [45]. Second, the nanoparticles act as strong reducing agents, and an excessive dose can drastically lower the system's redox potential beyond the optimal range for the microbial community, causing a metabolic shock and inhibiting their activity [46]. These observations are consistent with the phylum level microbial diversity analysis where *Bacillus sp*. were second dominated species after *Clostridium* species. (later discussed in section metagenomics analysis). Although, it was obserevd that the degradation efficiency of cellobiose and BSA increased from 92.25% to 97.24 % ($p<0.05$) and 47.25 % to 66.88% ($p>0.05$) respectively, the protein hydrolysis efficiency shows a variation due to presence of Ni/Fe_2O_3. The hydrolysis facilitates the cleavage of bonds in complex polysaccharides, protein, and lipids. Herein, variation in the abundance of genes encoding for group of enzymes such as Esterase (EC: 3.1.1) which acts on ester bond on complex lipids, Glycosidases (EC:3.2.1) facilitates the hydrolysis of O- and S- glycosyl bonds, and Protease (EC:3.4) were further investigated through COG and NOG, analysis, as discussed in section 3.4. These observed variances in gene abundances participating in hydrolysis signifying and strengthen the overall catalytic role of Ni/Fe_2O_3 that improves the hydrolysis of complex FW compared with control one by stimulating the hydrolytic efficacy of microbial consortium.

Nano Ni/Fe_2O_3, exhibits surface active ions and can interact with organic matter in both aqueous and non-aqueous phases, and which might cause a ionic and non-ionic interactions between hydrophilic organic such as in food waste [47]. Besides, the biological interaction of Ni/Fe_2O_3 Catalysts and the essential enzymes responsible for hydrolysis and solubilization, resulting in increased production of hydrolytic

View Article Online
DOI: 10.1039/D5SE01709B

enzymes, evidenced by metagenomic analysis. Similar reports on nano catalysts with FW have suggested that the Fe_2O_3 and NiO nanoparticles enhanced the activity of enzymes associated with hydrolysis such as proteases and alpha glycosidase in anaerobic biohydrogen process [48, 49]. The infrared spectrum (FTIR) was used for the assessment of various functional groups resulting from the presence of Ni/Fe_2O_3 in the FW based DF-system, as shown in Figure 1h. This FTIR assessment is performed for the samples taken from FW DF-system and annotated as control, and the system added 200 mg/L and 500 mg/L of Ni/Fe_2O_3 catalyst. The observed elongated peaks at 3000-3500 $cm^{-1,}$ were attributed to the O-H stretching vibrations, indicating the presence of water or hydroxy groups in the post-fermentative FW based DF-system. Where, the concomitant appearance of the peaks at 2924.76, 1653.62, 1156.55, 1241.07, 1053.50, 933.49, and 765.74 manifested the formation of C-H stretching vibrations, C=O and C=C vibrations, C-O-C and C-O stretch, , C-O-R stretch, S-O stretch, O-H bend (carboxylic acids) and cis=C-H vibrations, respectively (SI Table S1) which confirming the intercalations of aliphatic methylene, Aldehydes-carboxylates-aromatic skeleton, polysaccharides-phosphodiesters, inorganic sulfates, ether units, carboxylic acids and alkyl halides in the post fermented FW from DF-system [50]. The infrared peak of 1156 cm^{-1} (aromatic amines) was observed higher in the samples added with Ni/Fe_2O_3 than the control one. Besides, fluctuations in infrared peak of 921.49 cm^{-1} were also observed. Particularly, the decreased infrared peak band at 1156.55 cm-1(polysaccharides) and 933.49 (VFA) indicates the consumption of mono-molecules dissociated from the macromolecules and their subsequent degradation. The FT-IR behavior of this band is slightly different from FW sample added with Ni/Fe_2O_3, and it might be attributed to released metabolites in samples and enough to become visible in the spectrum, which signifies the enriched H_2-yield.

3.3 Ni/Fe_2O_3 mediated FW based DF biohydrogen production

The parametric variations in FW-based DF-system during H_2, the system's E_h and pH in response to exposure to Ni/Fe_2O_3 is shown in Figure 2c. The maximum E_h of 1971.5 mS/m detected in the fermentation system contains 500 mg/L of Ni/Fe_2O_3. Compared with the controlled DF-system (1202.5 mS/cm) the observed magnitude of E_h variation is significant ($p< 0.05$). The reason can be explained by the fact that adequate dispersion and when it is adequately applied to the surface then the E_h of the composite can be increased and resulting nanoparticles enrich the E_h to the biological systems. The electromagnetic interference of nanomaterials materials such as Ni and Fe_2O_3 and their composite reflect more effectively to improve E_h, therefore increasing E_h of biosystems. The pH of the DF-system as depicted in Figure 2c, is a crucial indicator revealing the metabolic shifting as well as microbial population shifting biosystems. The fluctuation in pH of spent medium was observed in response to varying concentration of Ni/Fe_2O_3. Although these variations were statistically not significant ($p>0.05$), an increased value of pH 4.9 was

View Article Online
DOI: 10.1039/D5SE01709B

observed to be the DF-system accompanied with 500 mg/L of Ni/Fe_2O_3 compared with control which accounted for 3.67.

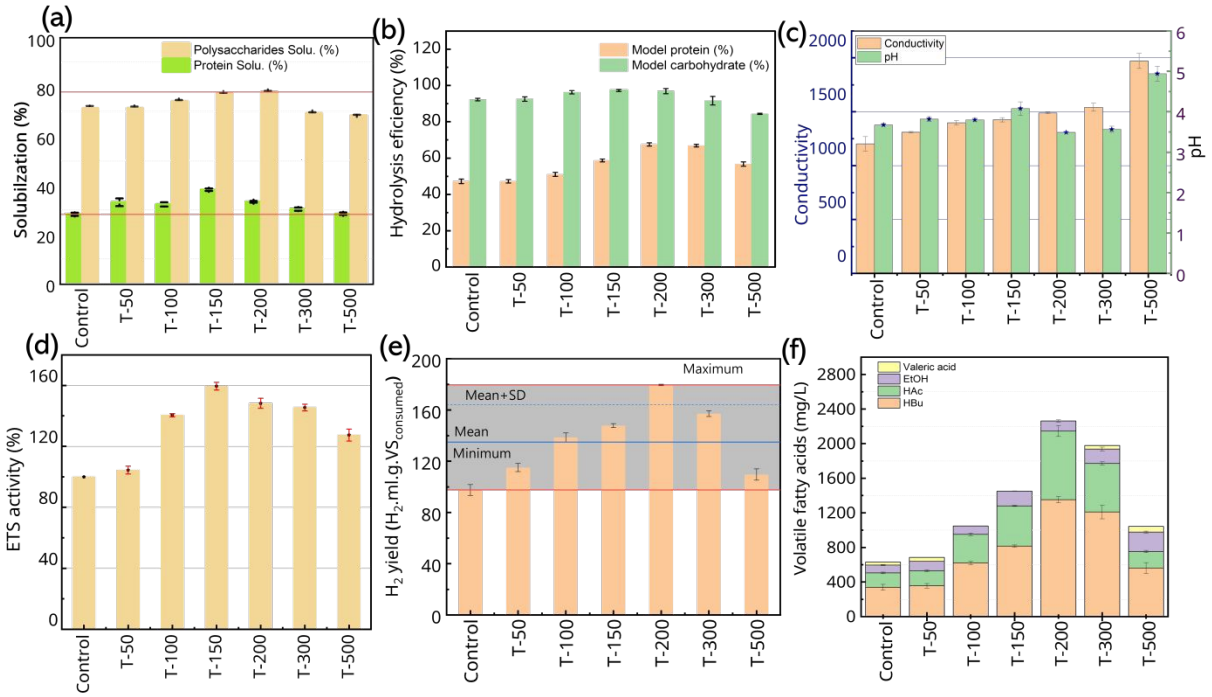

Figure 2. (a) Solubilization: Content of soluble polysaccharides and protein after fermentation (b) Hydrolysis: Content of consumed model protein and saccharides as model compound (p*, The sample test variance was statistically calculated using 'one sample Wilcoxon Signed rank (WSRT t-Test). (c) Conductivity and pH profile of spent medium (d) Electron transport system activity (e) Hydrogen yield profile (f) Soluble metabolites profile

The relationship between the E_h and the ions for the DF-based biohydrogen process is well known ($G=a*Hac + b*Hbu +c*Na^+ + d* HCO_3^- + G_0$; where, Na represents sodium ions concentration for a particular pH to regulate the system pH) [51]. Focusing on the H_2 yield of the hydrogen production system, at levels of 200 mg/L of Ni/Fe_2O_3 to the system, pH of the ceased DF-system varied from 3.61 to 3.49 and E_h from 1202.5 to 1428.5 mS^{-1}. This evidence shows that the augmentation of ions such as Ni^{2+}/Ni^{3+} and Fe^{2+}/Fe^{3+} applied Ni/Fe_2O_3 to DF-system is beneficial. It is suggested that controlling the E_h and pH of DF-system using Ni/Fe_2O_3 nanoparticles significantly lowers both the pH and conductivity compared to the control[52]. This leads to an increase in H_2 production, which is consistent with existing literature indicating that a reduction in system pH can enhance H_2 productivity[27, 53]. The electron transport system (ETS) activity assay reveals the microbial metabolic communities' activities in anaerobic respiration where dehydrogenases are used as terminal electron acceptor proceedings electron transfer steps [54] . The conducted ETS assessment shows the change of microbial metabolic activity in response to Ni/Fe_2O_3 to DF-system. As shown in Figure 2d, ETS activity positively correlates with the Ni/Fe_2O_3 doses, which is consistent with the production performance of H_2. Compared with, the ETS activity of the Ni/Fe_2O_3 added group (50, 100,

View Article Online
DOI: 10.1039/D5SE01709B

150, 200, 300, and 5000 mg/L) significantly ($p < 0.05$) increased by 04.37, 40.37, 59.45, 48.21, 45.48, and 27.42%, respectively. The trace metal ions have specific biochemical functions in the cell during the ETS-associated metabolic pathways and change its concentration alters the metabolic function. Herein, the presence of Ni^{2+}/Ni^{3+} and Fe^{2+}/Fe^{3+} in Ni/Fe_2O_3 exhibiting the increased potential to metabolic activity which is coordinated with the electron transport system. The presence of 150 mg/L Ni/Fe_2O_3 to the DF-system increases the electron transport activity assay up to 59.45% compared to control one. This could be explained as the presence of Ni^{+2} and Fe^{+2} ions could serve as electron acceptors following the reduction of Fe^{3+} to Fe^{2+} and Ni^{3+} to Ni^{2+} [55,56], and it might promote the ETS through multiple actions in DF-system.

Increments in H_2 yield in DF-system in response to different dose levels of Ni/Fe_2O_3 are observed and depicted in Figure 2e. The H_2 yield increases to 179.62 ml H_2.ml/g.$VS_{consumed}$ when the DF-system was supplemented with 200 mg/L of Ni/Fe_2O_3. Whereas, the system added Ni/Fe_2O_3>200mg/L shown the lowered H_2 yield. In the controlled DF-system (no Ni/Fe_2O_3 added), the H_2 yield of 97.57 ml H_2.ml/g.$VS_{consumed}$ was observed. The supplementation of Ni/Fe_2O_3 to the DF-system, significantly ($p<0.05$) increases the H_2 yield, as the doses of Ni/Fe_2O_3 increase from 50 to 200 mg/L, the H_2 yield increases from 115.09 to179.62 H_2.ml/g.$VS_{consumed,}$ which was an increase of 55.65% compared to the control. Besides, the further increase in Ni/Fe_2O_3 from 200 mg/L to 500 mg/L, a decline in H_2 yield from 179.62 to 109.63 H_2.ml/g.$VS_{consumed,}$ was observed. It is suggesting dwindling metabolic processes, and thus lowering the H_2 yield. The reason can also be explained by the fact that DF bacteria can quickly adapt to the environment augmented with Ni/Fe_2O_3 shown good $\mathbf{E_h}$ and enriched their metabolic pathway pathways in DF-system and thus increasing H_2 yield. Ni/Fe_2O_3 serve as electron acceptors for H_2 producing bacteria and leads to alteration in the electron transfer pathways, which not only prompts the production of extracellular polymeric substances but also increases the NADH/NAD^+ or $FADH_2$/FAD ratio[57]. Ni/Fe_2O_3 as nanocatalyst for growth and H_2 generation by adapting it depending on the type and concentrations of NPs has a unique adaptive ability. As in later section, we also observed the Ni/Fe_2O_3 and their effect at the genomic level and detected the abundancy of Clusters of Genes (COG) particularly hydrolase, FMN and NAD Oxidoreductase, along with Electron transports system enzymes, which directly influence the formation of ATP and H^+ gradients, and plays an important role to regulate [Fe-Ni] hydrogenases in the production of H_2 in DFHP process system. Soluble metabolite analysis suggested that the, when the dosage of Ni/Fe_2O_3 to DF-system increased from 50 to 200 mg/L, the C_2-H_{Ac}/C_4-H_{Bu} ratio increased 0.49 to 0.58 (Figure S2), while the further increase in doses of Ni/Fe_2O_3 to 500 mg/L the ratio decreases to 0.33. All the test groups exhibited a comparable molar ratio of C_2-H_{Ac}/C_4-H_{Bu} ranging from 0.490 to 0.586 and dominated proportion of C_4-$H_{Bu.}$ The higher concentration of C_4-H_{Bu} over C_2-H_{Ac} in the DF-system, suggests 'butyrate type of hydrogen production' metabolic pathway followed by microbial population [28, 58].

View Article Online
DOI: 10.1039/D5SE01709B

DF-system with Ni/Fe_2O_3 (200 mg/L) exhibited the higher C_2-H_{Ac}/C_4-H_{Bu} ratio of 0.58 and the control group with no Ni/Fe_2O_3 showed a comparatively lower molar ratio of C_2-H_{Ac}/C_4-H_{Bu} (0.485), which suggest the magnitude of C_4-H_{Bu} production is significant (p= 0.03). While no significant variation (p = 0.05) was observed in C_2-H_{Ac} production. In all these groups observed variations in EtOH concentrations were also significant (p = 0.04), increased to 225 mg/L (at 500 mg/L of Ni/Fe_2O_3) compared with control which accounted for 92 mg/L (no Ni/Fe_2O_3) The reduced degree of electron flow in the presence of EtOH has been reported for DF-system, which also justifies the lowered H_2 yield in this set of experiments[59]. In DF-system, VFAs are the key product of acidification from the ferments of FW [60, 61]. The effect of Ni/Fe_2O_3 dosages on H_2-yield and VFAs concentration emphasizes the efficacy of catalysts in improved FW fermentation in DF-system. The DF-system with optimal dose not only improves acidification but also results in improved H_2 yield at a significant level. The assessment of ETS and E_h [62], which had been used to assess total electron transport assay activity by the microbial population [63], and the observed H_2 yield correspondence with increased ETS supporting the catalytic behavior of Ni/Fe_2O_3. These observations are consistent with other previously reported studies where increased ETS and VFA produced from the bioconversion FW [64], involved syntropic electron transfer process, and iron and nickel nanoparticles and been reported to have the ability to mediate electron transfer between different guilds [65, 66]. In the current system significant enhancement evidence, the potential of Ni/Fe_2O_3 to increase ETS, E_h, and VFA, and might accelerate the electron transfer and thereby, increase overall H_2 yield in FW based DF-system.

3.4 Bioinformatics for Taxio-metagenomics

The microbial population and diversity analysis is evaluated using 16srRNA gene amplicons resolved into amplicon sequence variants (ASVs) reflecting a statistical difference in taxonomic alpha (Figure S3 SI) diversity between naïve (Control system) and DF-system added with 200 mg/L of Ni/Fe_2O_3 (Test System). The taxonomic and alpha diversity regression plot, (Figure S4 SI) revealed the higher abundance-based coverage estimator (ACE) index in Test System, which is supported by the higher Chao1 index. The H' and Simpson indices estimated diversity observed Pielou's evenness less significantly varied in the pair-wise comparison of these two samples on the basis of observed values of principle co-ordinate analysis, where the significance level observed by Tukey's HSD range test for H', Simpson and Pielou's evenness were 0.31, 0.31 and 0.31, respectively Figure S4 SI._The taxonomic composition from kingdom to species level in observed Test System, relative abundance of Genus *Clostridium* was dominated in both of the samples, Figure 3(a-f). Highlighting the Species-level diversity, *Clostridium beijerinckii*, *Clostridium LS* and *Clostridium chromiireducens* were the major species present in both types of system, but their proportions were influenced by the presence of Ni/Fe_2O_3. The increased proportions of *Clostridium*

View Article Online
DOI: 10.1039/D5SE01709B

beijerinckii from 63.16 to 64.21%, *Clostridium_LS* from 2.14 to F2.48% and *Clostridium_choromiireducers* from 1.23 to 1.55% were comparatively observed in Test System.

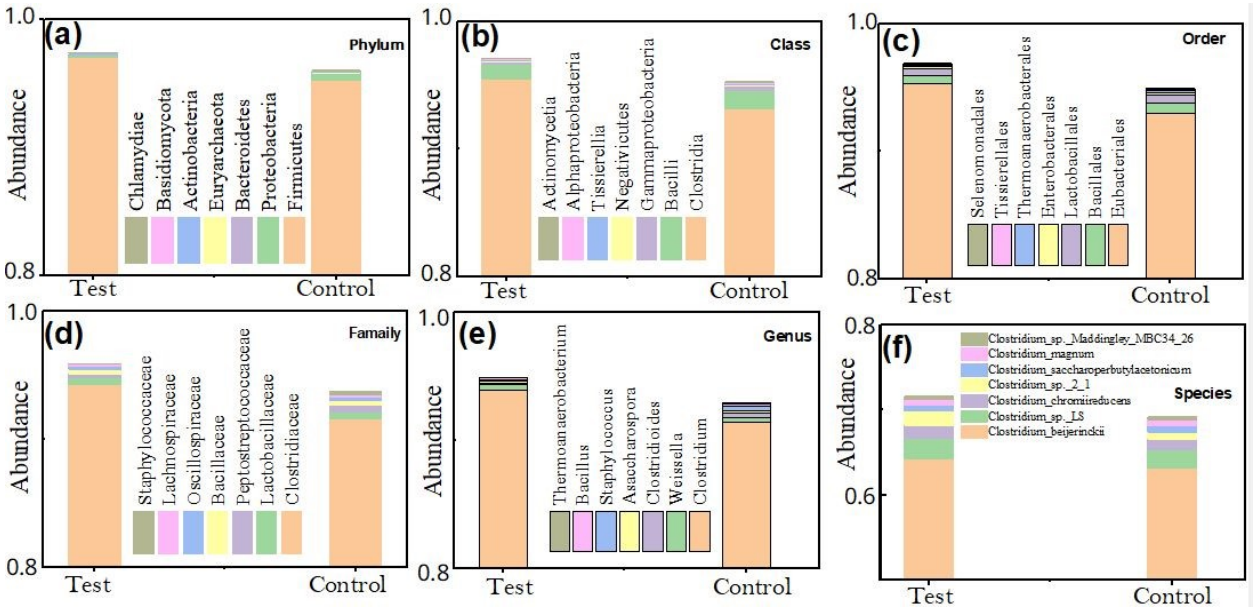

Figure 3. Taxonomic annotation, (a-f) Taxonomic shifts in microbial community structure in biohydrogen production systems in response to Ni/Fe_2O_3 supplemented to the anaerobic biohydrogen production system. From Phylum level observations to Species level.

The chord diagram of antibiotic resistance genes (ARGs), both the samples revealing the dominancy of Multidrug, Glycopeptide, Macrolide, Peptide and Fluoroquinolone resistance genes, Figure 4. The significant change observed in multidrug and Glycopeptide resistance genes between Test and Control System in response to Ni/Fe_2O_3 in DF-system. Most of the ARGs (34.3%) were present in both systems, while 39.5% and 26.2% of ARGS were observed uniquely in Test and Control samples, respectively. This suggested that the exposure microbial population to Ni/Fe_2O_3 Catalysts did lead to cross-border increase in the Test system. Thus, DF-system with Ni/Fe_2O_3 additive reclaimed more ARGs may help decrease diversity and abundance of ARGs in the system. Diversity richness and relative abundance in metagenomes reflect the dominant metabolism that there are characteristics functional profiles of the metagenomes. The Carbohydrate-Active Enzymes gene (CAZys) Family, an important from FW based DF-system is shown in Figure 5a, which highlighted the abundancy of Glycoside Hydrolases (GH), Glycosyl Transferases (GT), Polysaccharide Lyases (PL), Carbohydrate Esterase (CE), Auxiliary Activities (AA) and Carbohydrate-Binding Modules (CBM) genes (Figure S5 SI).

The parallelograms (Figure 5a) used for pairwise expression difference in CAZys gene abundance between Test and Control System, the variation in gene abundance is clearly depicted. It shows a

View Article Online
DOI: 10.1039/D5SE01709B

retrogression of GH3 and GT28 that particularly attack cellulose and backbones hemicellulose and help intracellular peptidoglycan synthesis, respectively. In contrast, the enrichment of CE1 and CE2 is a family of hydrolase enzymes that are involved in the hydrolysis of large variety of substrates, particularly the hydrolysis of O-linked acetyl groups from Xylan oligo- and polysaccharides, signifying the role of Ni/Fe_2O_3 in CAZys in FW based DF-system. These observations are consistent with reported literature where adsorption of ZnO-NPs evidence promote in abundance level of gene controlling the CAZys system in particular enzymatic glycosyltransferase and reported the key role of ZnO-NPs in biosynthetic genes in metabolic processes [67].

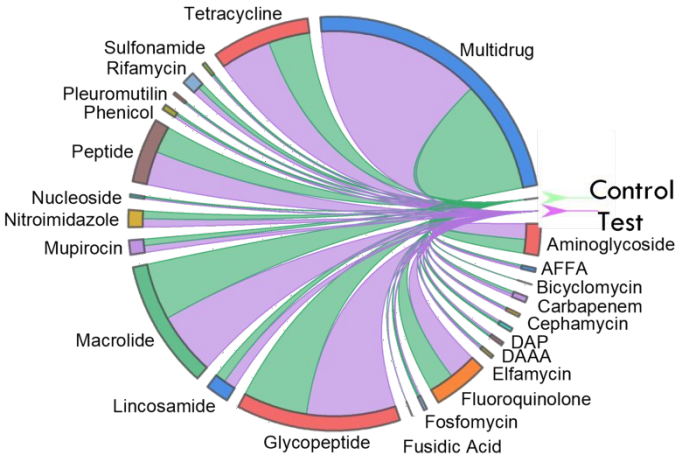

Figure 4. The abundance of antibiotic-resistant types representing observations for Test and control system. The width of the circular bar represents the total abundance of ARGs in each sample, Test and Control represents the anaerobic H_2 production system augmented with engineered nanoparticle of Ni/Fe_2O_3 and without Ni/Fe_2O_3 augmentation, respectively.

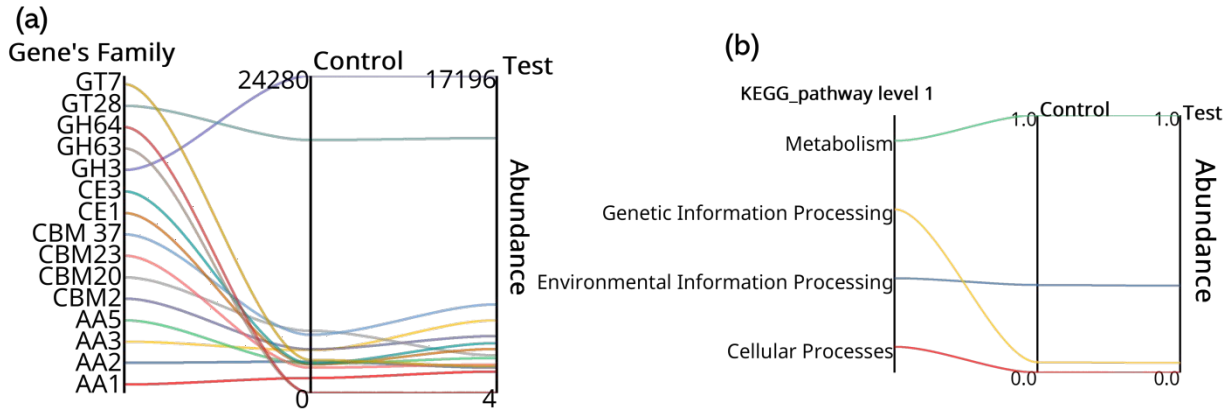

Figure 5. Functional annotation (a) relative content of corresponding functional gene number belongs to Carbohydrate-Active Enzymes gene (CAZy-family genes), and (b) the classification content at KEGG_Pathway_Level_1. Normalized abundance values of 0-1, Test and Control represent the anaerobic

View Article Online
DOI: 10.1039/D5SE01709B

H_2 production system augmented with engineered nanoparticle of Ni/Fe_2O_3 and without Ni/Fe_2O_3 augmentation, respectively.

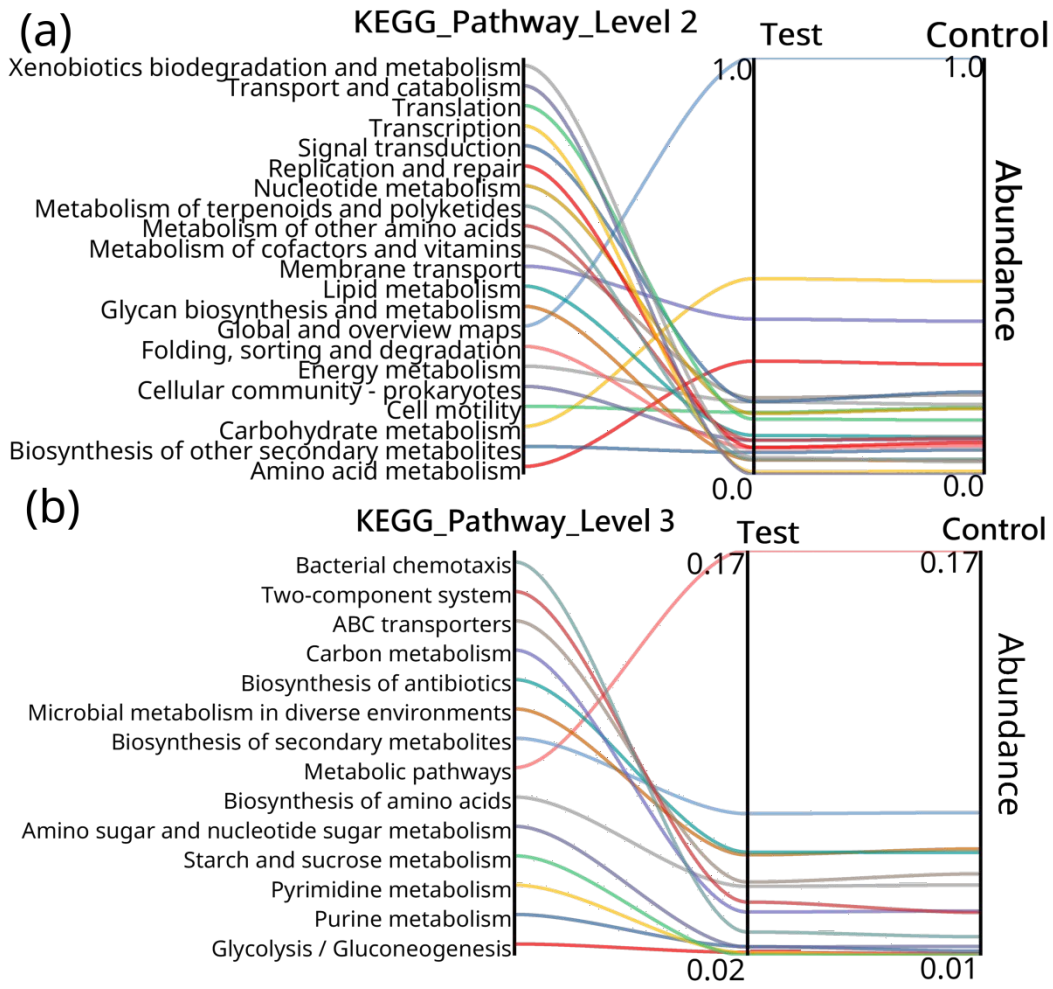

Figure 6. Functional annotation (a) relative content of corresponding functional gene number KEGG Pathway Level_2 and (b) the classification content at KEGG_Pathway_Level_3. Normalized abundance values of 0-1, Test and Control represent the DF-system augmented with engineered nanoparticle of Ni/Fe_2O_3 and without Ni/Fe_2O_3 augmentation, respectively.

In the functional annotations analysis, Metabolism, genetic information processing, cellular processes, and environmental process information systems were the dominant functions predicted at level one in the KEGG_Level_1 pathway in Figure 5b in both systems. The analysis of KEGG_Pathway_Level_2 (Figure 6a) functional categories within these Level_1 domains identified differences in metabolic potential between these two samples. Within level_2 Energy production and conversion, Amino acid transport and metabolism, Carbohydrate transport and metabolism domain, in DF-system with Ni/Fe_2O_3 the relative enrichment and abundance of sequences affiliated with Level 2 categories such as Xenobiotics

View Article Online
DOI: 10.1039/D5SE01709B

biodegradation and metabolism, carbohydrate metabolism, membrane transport, and amino acid metabolism were observed. By using specific functional information and analyzed for a differential abundance of KEGG level_3 pathways between Test and Control system, specific metabolic pathways could be identified, Figure 6b. Test system evidence abundances in Xenobiotics biodegradation and metabolism, carbohydrate metabolism, membrane transport, and amino acid metabolism in response to Ni/Fe_2O_3 into DF-system. These observed effects on amino acid metabolism are consistent with literature where Rui et al (2018) revealed that the presence of Fe-NPs increases the phylogenic system of Arachis hypogaea and so on increases the amnio acids metabolism[68]. Similar observations were reported by Garcia-Rodriguez et al., who described the role of Fe_2O_3 NPs in accelerating the membrane transport through brush border membrane enzymes through aminopeptidase-N (observed in this study) and Na^+/K^+ ATPase [69]. The changes in Cluster of Genes (COG) and Nonsupervised Orthologous Groups (NOG) categories in Figure 7 of gene clusters assigned DF-system metabolism aspects, which includes key regulation of Glycolysis, Kreb cycle and oxidative phosphorylation evidenced abundance richness in response to Ni/Fe_2O_3. One plausible explanation for this could the presence of Ni/Fe_2O_3 inferred the oxido-reductive pathways and hence the regulatory mechanism such as upregulation [4Fe-4s] ferredoxin and iron sulfur binding proteins, NADH dependent FMN reductase, Hydrogenase expression protein HypE, Hydrogenase maturation protein HypF, and electron transfer complex intermediates influenced. The NADH pathway is closely related to H_2 production, which is due to pyruvate production from a glucose molecule accompanied by NADH production. The coordinated association with upregulation of key metabolic enzymes related to hydrolysis (hydrolase, alpha amylase), solubilization (glycogen debranching enzymes), kinases and oxidoreductase; where the iron oxides NPs and its composite Ni/Fe_2O_3 facilities the kinases protein at expression levels and its association with iron-NPs and FAK protein and FAK-mediated signaling is being reported [70]. Herein the dose dependent catalytic effect of Ni/Fe_2O_3 is observed, where the FW based DF-system with 200 mg/L of Ni/Fe_2O_3 shown the accessible limit for the microbial communities to interact or improve hydrolysis capability which later improves conversion of complex macromolecules to soluble sugars, protein or lipids. This evident the dose dependent interaction between nanocatalysts and biological system and could be explained as intrinsic behavior of Ni/Fe_2O_3 that leads optimal physical adsorption [71] and the internalization or intracellular trafficking [72] of ions to the microbial consortium and subsequently increase the overall hydrolysis. Convincingly, the metagenomics analysis leads to a coordinated relationship between the Ni/Fe_2O_3 and metabolic pathway in microbiotas at molecular level, Figure 8. The upregulation of some key metabolic activity enzymes suggests a positive deviation from the control sample (no Ni/Fe_2O_3), to channelized H_2 production in FW based DF-system.

View Article Online
DOI: 10.1039/D5SE01709B

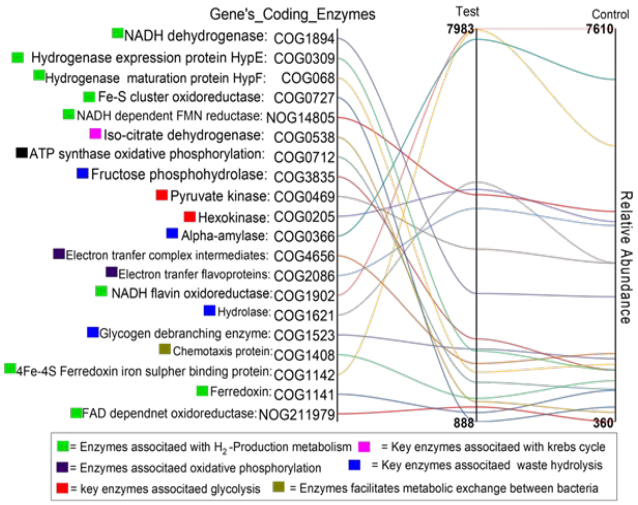

482

483 **Figure 7.** Parallelograms showing the abundance of COG and NOG category for the Test and Control
484 system.

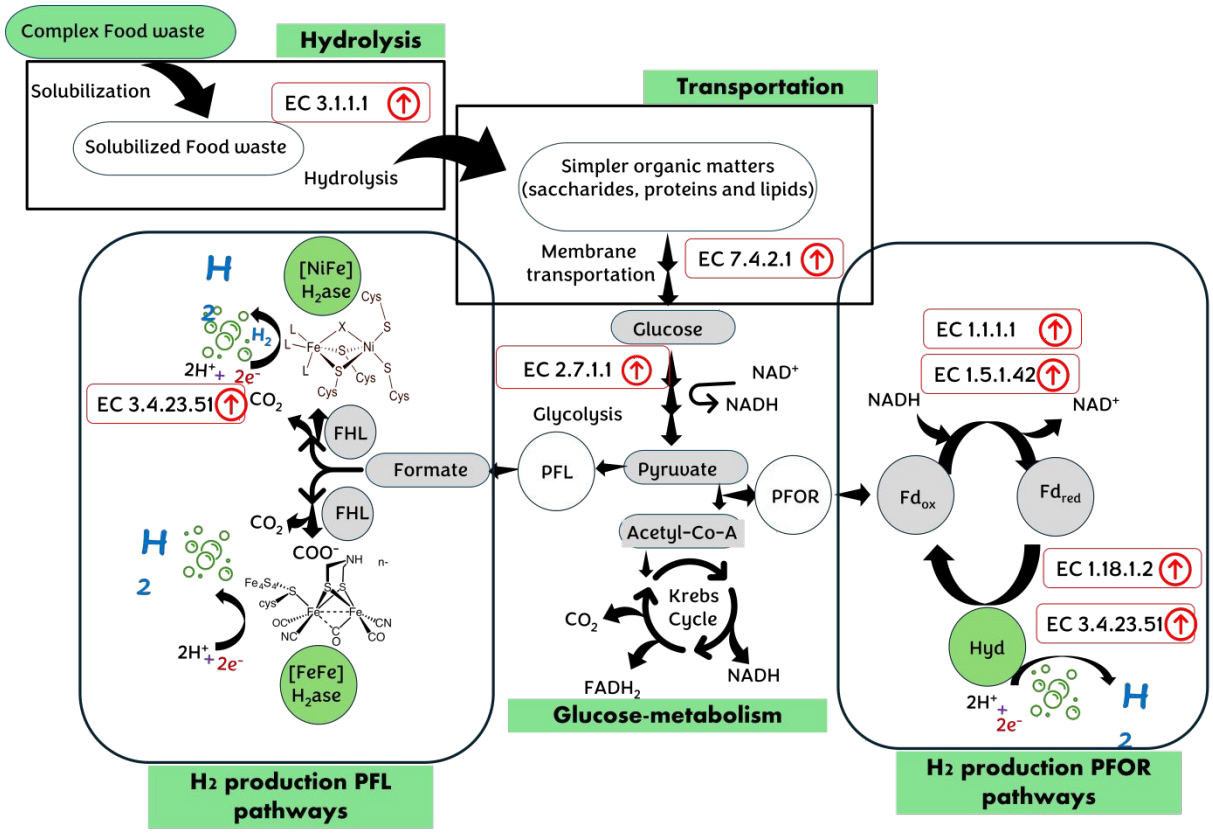

Annotations: PFOR: Pyruvate: ferredoxin oxidoreductase; PFL: pyruvate formate lyase; FHL: formate hydrogen lyase
Remakes: alpha amylase (3.1.1.1): facilitates the hydrolysis complex saccharides; ABC transporter proteins (7.4.2.1): facilitates transports of nutrients and other physiological substrates into bacterial cytoplasm; hexokinase (2.7.1.1): key enzyme of glycolysis which facilitate the phosphorylation of glucose; oxidoreductase (1.1.1.1): facilitates the electron transfer in $NAD^+ \leftrightarrow NADH$ system; 4Fe-4s ferredoxin (1.18.1.2): facilitates the electron transfer to ferredoxin;; NADH dependent FMN reductase (1.5.1.42): facilitates the reduction of NADH; Hydrogenase maturation proteins (3.4.23.51); facilitates the maturation of hydrogenase ([NiFe] hydrogenase).

485

View Article Online
DOI: 10.1039/D5SE01709B

Figure 8. Proposed mechanism for the impact of Ni/Fe_2O_3 engineered nanoparticles on anaerobic biohydrogen production at the metagenomic level. Red upward arrows indicate metabolic pathways and genes observed to be upregulated in this study. The Ni/Fe_2O_3 are hypothesized to enhance hydrogenesis by stimulating key enzymatic activities while also triggering microbial stress responses.

4. Conclusion

In conclusion, study synthesized a Ni/Fe_2O_3 nanocatalyst (200mg/L, 2.5 nm) and its parametric metagenomic effect on food waste-based batch fermentation was systematically investigated for biohydrogen production. It showed that, the catalyst enhanced hydrolysis, electron transport, conductivity, and short-chain fatty acid production, which favored the hydrogenotrophic pathway. Metagenomic analysis revealed the Clostridium species dominance and functional shifts: KEGG pathways showed enriched genes for genetic information processing, cellular processes, and environmental systems. Specifically, genes increased for saccharide hydrolysis enzymes, nutrient transport, glycolysis phosphorylation, and NADH/ferredoxin electron transfer (including Ni-Fe hydrogenase maturation). These findings demonstrated a novel genomic-level impact of bimetallic nanocatalysts in modulating microbial metabolism for efficient FW-based DF-system.

Declaration of competing interest

The authors declare that they have no competing interests.

Author contributions

The manuscript was written through the contributions of all authors.

Data availability

All the data and findings needed to evaluate the conclusions are present in the paper and supplementary section.

Acknowledgement

Thanks to the support of Hong Kong Environment and Conservation Fund (127/2022).

References

1. K. He, W. Li, L. Tang, W. Li, S. Lv and D. Xing, *Environmental Science & Technology*, 2022, **56**, 11931-11951.
2. P. Mishra, PhD thesis, Universiti Malaysia Pahang, 2018.
3. P. Mishra, PhD Thesis, , Universiti Malaysia Pahang, Malaysia, 2018.
4. P. Packiyadhas, S. K. Sivaperumal and S. Murugesan, *Journal of Material Cycles and Waste Management*, 2025, **27**, 777-795.
5. S. Wang, L. Peng, Y. Jiang, P. Gikas, B. Zhu and H. Su, *Sci Rep*, 2016, **6**, 34640.
6. E. B. Agyekum, M. I. Al-Maaitah, P. Kumar, F. Odoi-Yorke and F. L. Rashid, *Energy Conversion and Management: X*, 2025, **27**, 101111.
7. P. Mishra, D. Johnravindar, J. W. Wong and J. Zhao, *Sustainable Energy & Fuels*, 2022, **6**, 5425-5438.

View Article Online
DOI: 10.1039/D5SE01709B

8. J. d. J. s. Montoya-Rosales, A. Ontiveros-Valencia, D. A. Esquivel-Hernández, C. Etchebehere, L. B. Celis and E. Razo-Flores, *Environmental Science & Technology*, 2023, **57**, 11552-11560.
9. R. K. Thauer, K. Jungermann and K. Decker, *Bacteriological reviews*, 1977, **41**, 100-180.
10. A. P. Sohale, S. Janardanan, D. Yadav, B. Dash and M. D. Yadav, *Industrial & Engineering Chemistry Research*, 2023, **62**, 14755-14771.
11. Q. Kang, D. Lai, W. Tang, Q. Lu and F. Gao, *Chemical Science*, 2021, **12**, 3818-3835.
12. T. Luo, Q. Xu, W. Wei, J. Sun, X. Dai and B.-J. Ni, *Environmental Science & Technology*, 2022, **56**, 3658-3668.
13. B. Karthikeyan and G. Velvizhi, *International Journal of Hydrogen Energy*, 2024, **52**, 536-554.
14. D. Wang, Q. Pan, J. Yang, S. Gong, X. Liu and Y. Fu, *Environmental Science & Technology*, 2024, **58**, 2598-2614.
15. T. Manutsyan, S. Blbulyan, A. Vassilian, T. Semashko, G. Kirakosyan, L. Gabrielyan, K. Trchounian and A. Poladyan, *FEMS Microbiology Letters*, 2024, **371**, fnad138.
16. Y. Wang, Y. Zhao, S. Wang, G. Xiao, Y. Jin, Z. Wang and H. Su, *ACS Sustainable Chemistry & Engineering*, 2022, **11**, 300-311.
17. S. Kumar and P. Maiti, *Rsc Advances*, 2016, **6**, 67449-67480.
18. Z. Ji, H. Zhang, H. Liu, O. M. Yaghi and P. Yang, *Proceedings of the National Academy of Sciences*, 2018, **115**, 10582-10587.
19. W. Tu, I. P. Thompson and W. E. Huang, *Proceedings of the National Academy of Sciences*, 2024, **121**, e2404958121.
20. Ö. B. Gökçek and Ş. N. Erdoğmuş, *International Journal of Hydrogen Energy*, 2024, **49**, 337-348.
21. M. Taherdanak, H. Zilouei and K. Karimi, *International Journal of Hydrogen Energy*, 2016, **41**, 167-173.
22. R. Lin, J. Cheng, L. Ding, W. Song, M. Liu, J. Zhou and K. Cen, *Bioresource technology*, 2016, **207**, 213-219.
23. Z. Li, J. Wang, K. Tian, C. Zhou, Y. Pei, J. Zhang and L. Zang, *ACS omega*, 2022, **7**, 41594-41605.
24. C. Roy, B. Sebok, S. Scott, E. Fiordaliso, J. Sørensen, A. Bodin, D. Trimarco, C. Damsgaard, P. Vesborg and O. Hansen, *Nature Catalysis*, 2018, **1**, 820-829.
25. Q. Zhang, S. Xu, Y. Li, P. Ding, Y. Zhang and P. Zhao, *Fuel*, 2021, **305**, 121585.
26. W. Lubitz, H. Ogata, O. Rudiger and E. Reijerse, *Chemical reviews*, 2014, **114**, 4081-4148.
27. J. Yang, H. Zhang, H. Liu, J. Zhang, Y. Pei and L. Zang, *Bioresource Technology*, 2022, **351**, 127027.
28. P. Mishra, I. R. Akaniro, R. Zhang, P. Wang, Y. Geng, D. Li, Q. Xu, J. W. Wong and J. Zhao, *ACS ES&T Engineering*, 2024.
29. F. Ndayisenga, Z. Yu, B. Wang, G. Wu and H. Zhang, *Energy Conversion and Management: X*, 2024, **22**, 100541.
30. B. Xiao and J. Liu, *Chinese Science Bulletin*, 2009, **54**, 2038-2044.
31. A. S. Oberoi, S. Sriram and J. W. Wong, *International Journal of Hydrogen Energy*, 2024, **67**, 566-576.
32. W. Xiu, M. Wu, S. L. Nixon, J. R. Lloyd, N. M. Bassil, R. Gai, T. Zhang, Z. Su and H. Guo, *Environmental Science & Technology*, 2022, **56**, 10105-10119.
33. A. P. H. Association, *Standard methods for the examination of water and wastewater*, American public health association., 1926.
34. M. Gong, Y. Li, H. Wang, Y. Liang, J. Z. Wu, J. Zhou, J. Wang, T. Regier, F. Wei and H. Dai, *J. Am. Chem. Soc.*, 2013, **135**, 8452-8455.
35. J. Alsarraf, A. A. Al-Rashed, A. A. Alnaqi and A. S. Goldanlou, *Powder Technology*, 2021, **379**, 537-546.
36. M. W. Louie and A. T. Bell, *J. Am. Chem. Soc.*, 2013, **135**, 12329-12337.
37. H. Liang, M. Xu, Y. Bu, B. Chen, Y. Zhang, Y. Fu, X. Xu and J. Zhang, *Applied Surface Science*, 2019, **485**, 64-69.
38. Q. Luo, Y. Zhao, L. Sun, C. Wang, H. Xin, J. Song, D. Li and F. Ma, *Chemical Engineering Journal*, 2022, **437**, 135376.
39. A. P. Grosvenor, M. C. Biesinger, R. S. C. Smart and N. S. McIntyre, *Surface science*, 2006, **600**, 1771-1779.
40. P. Dubey, N. Kaurav, R. S. Devan, G. Okram and Y. Kuo, *RSC advances*, 2018, **8**, 5882-5890.
41. T. Yamashita and P. Hayes, *Applied surface science*, 2008, **254**, 2441-2449.
42. P. Li, Y. Xuan, B. Jiang, S. Zhang and C. Xia, *Electrochemistry Communications*, 2022, **134**, 107188.
43. L. Sun, C. H. Hendon, S. S. Park, Y. Tulchinsky, R. Wan, F. Wang, A. Walsh and M. Dincă, *Chemical science*, 2017, **8**, 4450-4457.

View Article Online
DOI: 10.1039/D5SE01709B

44. T. Raj, K. Chandrasekhar, R. Morya, A. K. Pandey, J.-H. Jung, D. Kumar, R. R. Singhania and S.-H. Kim, *Bioresource technology*, 2022, **360**, 127512.
45. S. Eduok, B. Martin, R. Villa, A. Nocker, B. Jefferson and F. Coulon, *Ecotoxicology and Environmental Safety*, 2013, **95**, 1-9.
46. P. Szczyglewska, A. Feliczak-Guzik and I. Nowak, *Molecules*, 2023, **28**, 4932.
47. L. Zhu, H. Tao, X. Dai, B. Dong and W. Zhang, *Journal of Environmental Management*, 2023, **326**, 116722.
48. Q. Wang, K. Feng and H. Li, *Bioresource technology*, 2020, **315**, 123804.
49. N. Srivastava, A. Hussain, D. Kushwaha, S. Haque, P. Mishra, V. K. Gupta and M. Srivastava, *Fuel*, 2021, **304**, 121391.
50. R. Posmanik, C. M. Martinez, B. Cantero-Tubilla, D. A. Cantero, D. Sills, M. J. Cocero and J. W. Tester, *ACS Sustainable Chemistry & Engineering*, 2018, **6**, 2724-2732.
51. C.-A. Aceves-Lara, E. Latrille, T. Conte and J.-P. Steyer, *Water Science and Technology*, 2012, **65**, 1281-1289.
52. P. Chen, Y. Wang, L. Yan, Y. Wang, S. Li, X. Yan, N. Wang, N. Liang and H. Li, *Biological research*, 2015, **48**, 1-8.
53. T.-H. Kim, D. Song, Y.-J. Jeon, O. Hwang, J.-Y. Nam and Y.-M. Yun, *Chemical Engineering Journal*, 2023, **476**, 146520.
54. K. Ma, H. Zhao, C. Zhang, Y. Lu and X.-H. Xing, *International journal of hydrogen energy*, 2012, **37**, 15875-15885.
55. S. Zhang, X. Zhang, Y. Yuan, K. Li and H. Liu, *Science of The Total Environment*, 2023, **855**, 158911.
56. S. Srikanth and S. V. Mohan, *RSC advances*, 2012, **2**, 6576-6589.
57. V. Schirrmacher, *Biomedicines*, 2020, **8**, 526.
58. F. Monlau, E. Trably, A. Barakat, J. Hamelin, J.-P. Steyer and H. Carrere, *Environmental science & technology*, 2013, **47**, 12591-12599.
59. W. Li, Q. Zhang, J. Liu, N. Ren, X. Zeng and Y. Jia, *Chemical Engineering Journal*, 2023, **474**, 145997.
60. G. Mohanakrishna, N. P. Sneha, S. M. Rafi and O. Sarkar, *Science of The Total Environment*, 2023, **888**, 163801.
61. M. Du, X. Liu, C. Li, S. Long, L. Luo, Y. Guo and D. Wang, *ACS ES&T Engineering*, 2023, **3**, 1986-1996.
62. J. Yang, Y.-B. Sim, H.-H. Joo, O. Mašek and S.-H. Kim, *International Journal of Hydrogen Energy*, 2024, **53**, 1293-1302.
63. J. Bu, H.-L. Wei, Y.-T. Wang, J.-R. Cheng and M.-J. Zhu, *Water Research*, 2021, **202**, 117440.
64. Q. Jiang, Y. Chen, S. Yu, R. Zhu, C. Zhong, H. Zou, L. Gu and Q. He, *Chemical Engineering Journal*, 2020, **398**, 125643.
65. Y. Zhu, Z. Zhao, Y. Yang and Y. Zhang, *Waste Management*, 2020, **118**, 481-490.
66. C. G. Camacho and B. Ruggeri, *Chemical Engineering Transactions*, 2018, **64**, 391-396.
67. M. Xiao, A. Li, X. Zhang and B. Ji, *Journal of Cleaner Production*, 2024, **447**, 141509.
68. M. Rui, C. Ma, J. C. White, Y. Hao, Y. Wang, X. Tang, J. Yang, F. Jiang, A. Ali and Y. Rui, *Environmental Science: Nano*, 2018, **5**, 2088-2102.
69. A. García-Rodríguez, F. Moreno-Olivas, R. Marcos, E. Tako, C. N. Marques and G. J. Mahler, *Environmental Science: Nano*, 2020, **7**, 3940-3964.
70. S. J. Soenen, N. Nuytten, S. F. De Meyer, S. C. De Smedt and M. De Cuyper, *Small*, 2010, **6**, 832-842.
71. X. Duan and Y. Li, *Small*, 2013, **9**, 1521-1532.
72. F. Zhao, Y. Zhao, Y. Liu, X. Chang, C. Chen and Y. Zhao, *small*, 2011, **7**, 1322-1337.

View Article Online
DOI: 10.1039/D5SE01709B

Data availability

All the data and findings needed to evaluate the conclusions are present in the paper and supplementary